

Nonlinear Dynamics Analysis of Electric Energy Regeneration Device Based on Vibration Energy Recovery



Wei Wang, Yan Li, Kehong Wu, Yongjie Cui, and Yuling Song

1 Introduction

The energy crisis has attracted more and more attention to energy-saving and environmentally friendly technologies, and related research on vibration energy recovery of electric vehicles has become a current research hotspot [1]. At present, research scholars mainly carry out research on energy recovery devices for vehicle suspension systems [2, 3]. The feasibility of energy recovery for the shock absorber has been studied and analyzed [4]; a variety of different types of devices have been proposed based on the vehicle's suspension system.

Taghavifar [2] researched the recovery of vibration energy of off-road vehicles, mainly considering the suspension system based on hybrid electromagnetic, and combined with the circuit dynamics of the electromagnetic energy recovery system to analyze the effectiveness of energy recovery. Through the acceleration response of chassis in the frequency domain and time domain, the influence of the vibration energy recovery system on driver/passenger riding comfort is studied and analyzed. Li et al. [5] proposed a new vibration energy collecting suspension system based on a generator and ball screw mechanism. Vehicle vibration energy is collected

W. Wang · Y. Li · K. Wu · Y. Cui

College of Mechanical and Electronic Engineering, Northwest A&F University, Yangling, Shaanxi, China

Y. Song (✉)

College of Mechanical and Electronic Engineering, Northwest A&F University, Yangling, Shaanxi, China

Key Laboratory of Agricultural Internet of Things, Ministry of Agriculture, Yangling, Shaanxi, China

Key Laboratory of Agricultural Information Perception and Intelligent Services, Yangling, Shaanxi, China

from the suspension system, and stored in the battery. Zhang et al. [3] integrated an arm-tooth drive electric energy regeneration device based on the vehicle suspension system to obtain a more accurate power output response. Through the 1/4, 1/2, and full-vehicle electric energy regeneration system models reveal the influence of road unevenness on the system power output. Unlike the above method, vibration energy recovery by functional materials has great advantages for small-amplitude vibration. Tavares and Ruderman [6] used piezoelectric ceramics to convert mechanical energy into electrical energy. The piezoelectric ceramic sensor's ability and efficiency of electric energy regeneration under two different types of external excitations are studied. Genovese et al. [7] studied the recovery of wasted energy from the vibration of train air suspension, design and develop an energy collection system integrated into a pneumatic spring. The boundary volume of the new equipment is defined mainly through reverse engineering technology, and the energy is collected by means of a resonance system and a temporary conversion mechanism located in a defined enclosed space.

On the basis of existing research, this paper proposes an electromechanical energy regeneration device with two one-way clutches for the reduction vibration of the power battery pack of an electric vehicle and extending the cruising range of electric vehicles. The transmission system in this device converts the two-way vibration of the rack into one-way rotation of the input shaft of the generator, thereby greatly improving reliability and efficiency. The generator will be driven in one direction to convert kinetic energy into electrical energy. In the movement process, the meshing of gears and racks, the transmission of bevel gears, the working process of a one-way clutch, and the process of contact, paired contact impact and separation processes occur at all times. In theory, chaos may occur in the system, which will lead to the decline of the motion stability of the electric energy regeneration device. The stability of system motion depends on whether the design of key parameters in the device is reasonable [8–10]. Many researches have been conducted on the influence of gear transmission system design parameters on performance.

Yang et al. [11] established a one-DOF gear pair model including time-varying meshing stiffness, static transmission error, and nonlinear backlash, and analyzed the stability of the gear system to obtain stable and unstable boundary conditions of the area. Finally, a parameter study is carried out to reveal the influence of several key parameters on the system performance. Xiao et al. [12] installed a dumbbell-shaped damper in the damping hole. Based on the nonlinear energy dissipation mechanism, the damping force is used as an external excitation and its damping effect is discussed. Using the dynamic coupling method of continuum and discontinuity, the equivalent displacement mapping of the contact load from the discontinuous domain of the gear to the node of the continuous element is realized. Zhu et al. [13] established the nonlinear dynamic model of the segmented bending and pendulum of the gear transmission system and studied its nonlinear dynamic characteristics and dynamic characteristics. Based on three different Poincaré maps, defined by bifurcation diagram, Lyapunov exponent diagram, phase diagram, and dynamic change curve, the effects of the load factor, meshing frequency, comprehensive transmission error on system dynamics and nonlinear dynamics are studied. Shin and Palazzolo [14] proposed a new method for modeling and analyzing

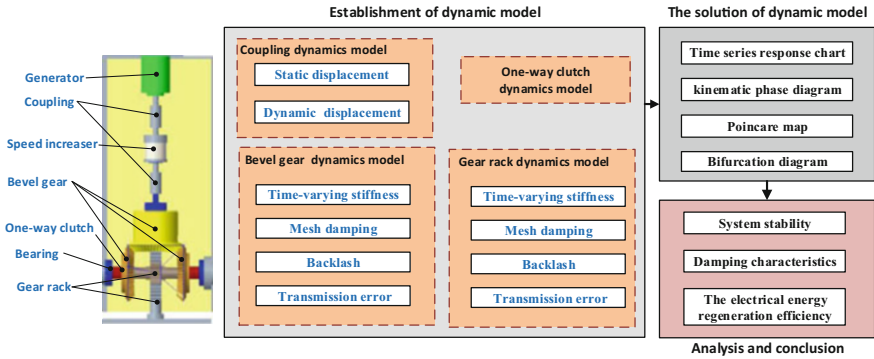


Fig. 1 Flow chart of nonlinear dynamic analysis of electric energy regeneration device

gear rotor-bearing systems. Considering the nonlinear force in the gear set and the supporting liquid film journal bearing, a rotor dynamic model with five degrees of freedom is established. Yi et al. [15] proposed a new nonlinear dynamic model of the spur gear system, which considered the time-varying behavior of pressure angle and gear clearance, as well as the influence of gear gravity, unbalanced mass, and internal/external excitation. The motion equation of the system is derived strictly by the Lagrange method and solved by the numerical integration method.

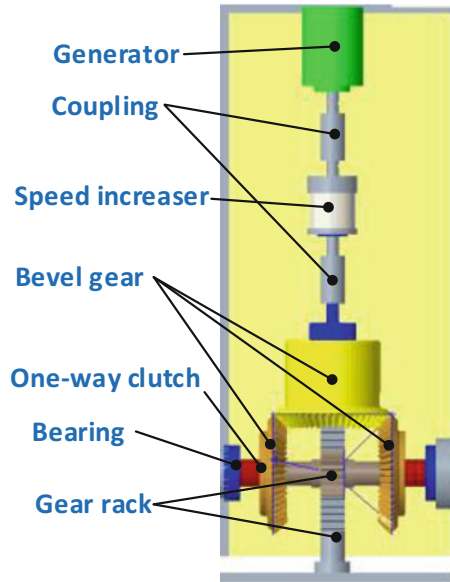
To sum up, this paper proposes a mechanical electromagnetic electric energy regeneration device. The layout design of two one-way clutches transforms the reciprocating vibration into a one-way rotation of the generator. In order to improve the motion stability of the electric energy regeneration device, the analysis of the nonlinear parameters in the device, considering the time-varying meshing stiffness, meshing damping, tooth side clearance, comprehensive transmission error of the meshing pair, and the reserve clearance of the one-way clutch. The mass concentration method is used to establish a multi-degree-of-freedom nonlinear dynamic model. The effects of excitation frequency, reserve gap, and integrated transfer error on the nonlinear dynamic performance were analyzed by time-series response diagrams, phase diagrams, Poincaré diagrams, and bifurcation diagrams, revealing the law of influence of parameters on the damping characteristics of the device. The research will lay a profound theoretical foundation and practical significance for improving the stability of the power regeneration system. Figure 1 shows the technical route studied in the paper.

2 Dynamic Model of Electric Energy Regeneration Device

2.1 Device Structure Design

This paper proposes an electromagnetic electric energy regeneration device using two one-way clutches. As shown in Fig. 2, it mainly has four parts: a rack and pinion

Fig. 2 Schematic diagram of electromagnetic energy regeneration device structure



mechanism, a bevel gear transmission mechanism, a generator, and an electric energy storage module. When an electric vehicle is driving on a road, the unevenness of the road elevation will cause a vibration of the electric vehicle. In order to alleviate the vibration of the battery pack, an electric energy regeneration device is installed between the battery pack and the chassis of the electric vehicle. The function of the rack and pinion transmission mechanism is to convert the relative linear motion between the battery pack and the chassis into the rotational motion of the generator. The bevel gear transmission mechanism includes two one-way clutches and three bevel gears. Its function is to convert the bidirectional rotation of the gears in the rack and pinion mechanism into unidirectional rotation of the bevel gears and drive the speed increaser and generator to rotate in one direction so that the generator can output electricity. The electric energy storage module is directly connected to the generator and contains three components of the filter circuit, voltage stabilizing circuit, and supercapacitor. The purpose is to store the electrical electric energy by the electrical energy regeneration system to increase the mileage of electric vehicles. The device can recover energy from vibrations with a large range of amplitude, effectively improve the cruising range of electric vehicles, take into account the safety of the power battery pack, and increase the rate of the energy regeneration and vibration energy recovery of the device.

2.2 Road Incentive and Time Domain Description

In the design process of the electric energy regeneration device, not only the strength and rigidity of the components must be considered, but also the vibration caused by

the unevenness of the road during the road driving process [16, 17]. The unevenness of the road is unpredictable, and the excitation to the car body is random, belonging to random loads. This kind of load cannot be used to express the load time history with a function, but this relationship can be described by statistics and probability theory. Bearing this kind of random load for a long time may cause large vibrations in the electrical energy regeneration device, which may affect the safety of the power battery pack and may cause cracks or fractures in the structure due to fatigue, shortening the service life of the device as a whole [18, 19].

The external excitation of the device comes from the unevenness of the road elevation. When performing device simulation research and performance evaluation, it is necessary to obtain accurate road information. The road unevenness input of vehicle vibration mainly adopts the form of road power spectrum density. The most direct method to obtain the road surface spectrum is measurement, but it is laborious, time-consuming, and uneconomical. Many scholars have measured road surface unevenness and determined that the power spectrum density function and variance of the road surface describe its statistical characteristics. In 1984, the International Organization for Standardization put forward the “Draft Representation Method for Descriptive Roughness” in the document ISO/TC108/SC2N67. China also formulated the corresponding national standards by referring to it. The Changchun Automobile Research Institute drafted and formulated GB/T7031-1986 “Vehicle Vibration Input-Standard for Road Surface Roughness Representation Method. The formula (1) is used in the documents to fit and describe the road power spectrum density [17].

$$G_q(n) = G_q(n_0) \left(\frac{n}{n_0}\right)^{-w} \tag{1}$$

where n is spatial frequency, n_0 is reference spatial frequency, $G_q(n_0)$ is the road power spectral density at the reference spatial frequency, and $G_q(n)$ is the road roughness coefficient. w is the frequency index, which is the slope of the diagonal line in double logarithmic coordinates and usually takes the value of 2. The document divides the road into eight classes, and in this paper, we mainly use class D road for the study. The roughness coefficient of class D road is $1024 \times 10^{-6} \text{ m}^3$, and the root mean square value is $30.45 \times 10^{-3} \text{ m}$.

There is no speed influence factor present in the spatial frequency power spectrum description. But for vehicle vibration systems, the vehicle speed is a factor that must be considered [18]. When a car travels on a road surface with a spatial frequency n at speed u , the equivalent time-frequency is $f = un$.

Therefore, the time-frequency power spectral density is

$$G_q(f) = \frac{1}{u} G_q(n_0) \left(\frac{n}{n_0}\right)^{-w} = G_q(n_0) n_0^2 \frac{u}{f^2} \tag{2}$$

Since the road surface is regarded as a superposition of a group of sine waves with different wavelengths, amplitudes, and phases, it can be assumed that the spatial frequency range of the group of waves is (n_1, n_2) and the interval (n_1, n_2) is divided

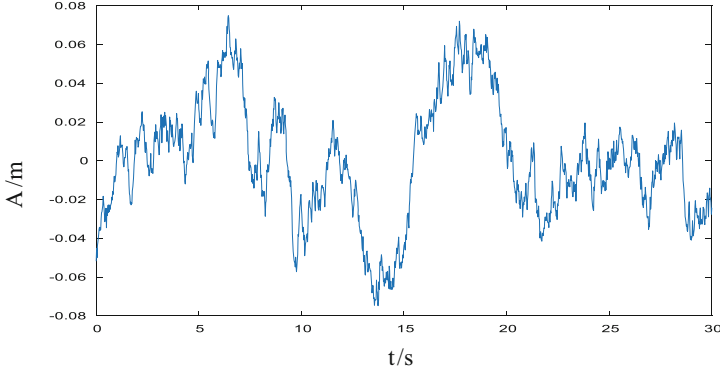


Fig. 3 Time-domain displacement excitation for class D road ($u = 5$ m/s)

into N cells. The center frequency between i th cell is $n_{\text{mid-}i}$, the interval width is $\Delta n = (n_2 - n_1)/N$, then the corresponding road surface displacement power spectrum density is:

$$G_q(f_i) = G_q(n_0) n_0^2 \frac{1}{un_{\text{mid-}i}^2} \tag{3}$$

Therefore, the expression of the sine signal corresponding to this interval is

$$\sqrt{2G_q(f_i)} \Delta n \sin(2\pi un_{\text{mid-}i}x + \alpha_i) \tag{4}$$

As shown in Fig. 3, multiple sine signal waveforms are superimposed to obtain an expression for the random excitation of farm pavements:

$$q(x) = \sum_{i=1}^N \sqrt{2G_q(f_i)} u \Delta n \sin(2\pi un_{\text{mid-}i}x + \alpha_i) \tag{5}$$

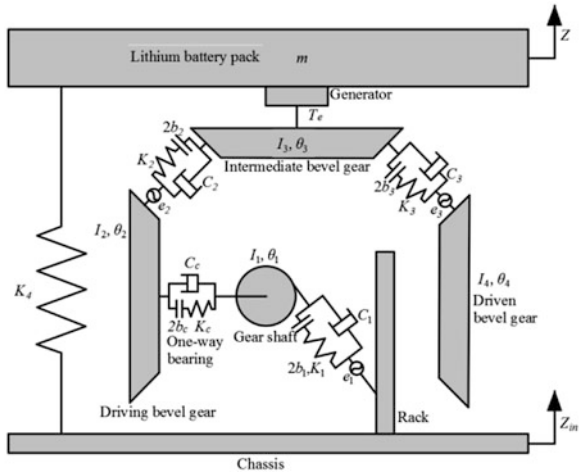
where α_i is a random number uniformly distributed in $[0, 2\pi]$. In this study, the first harmonic term of the road displacement excitation is selected, and the time domain road displacement excitation is:

$$q(t) = A \sin(\omega t + \phi) \tag{6}$$

2.3 System Dynamics Model

The dynamic model of the mechanical electromagnetic power regeneration system is shown in Fig. 4. In the figure, Z_{in} is the displacement excitation of the soil road

Fig. 4 Dynamic model of electric energy regeneration device



surface; Z is the vertical displacement of the lithium battery pack; and r_i, I_i, θ_i ($i = 1,2,3,4$) are the base radius, inertia, and angular displacement of torsional vibration of the gear, respectively. C_1, K_1, b_1 , and e_1 are the meshing damping, time-varying meshing stiffness, tooth side clearance, and comprehensive transmission error of the rack and pinion meshing pair respectively. C_i, K_i, b_i , and e_i ($i = 2,3$) are the meshing damping, time-varying meshing stiffness, tooth side clearance, and comprehensive transmission error of the i th gear meshing pair respectively. C_c, K_c, b_c are the torsional damping, torsional stiffness, and reserve clearance when the one-way clutch is in contact. T_e is the induced torque generated during the operation of the generator.

Considering the time-varying meshing stiffness, meshing damping, tooth side clearance, and comprehensive transmission error of the meshing pair, as well as the reserve clearance of the one-way clutch, the mass concentration method [20] is used to establish the nonlinear vibration equation of the dynamic model shown in Fig. 4 as

$$\begin{cases} I_1\ddot{\theta}_1 = r_1(K_1f_1 + C_1\dot{X}_1) - K_cfc - C_c\dot{X}_c \\ I_2\ddot{\theta}_2 = K_cfc + C_c\dot{X}_c - r_2(K_2f_2 + C_2\dot{X}_2) \\ I_3\ddot{\theta}_3 = r_3(K_2f_2 + C_2\dot{X}_2) - r_3(K_3f_3 + C_3\dot{X}_3) - T_e \\ I_4\ddot{\theta}_4 = r_4(K_3f_3 + C_3\dot{X}_3) \\ m\ddot{Z} = K_4X_4 + K_1f_1 + C_1\dot{X}_1 \end{cases} \quad (7)$$

Among them, the relative displacement of each meshing pair is:

$$\begin{cases} X_1 = Z_{in} - r_1\theta_1 - Z \cos \alpha - \bar{e}_1 \\ X_c = \theta_1 - \theta_2 \\ X_2 = r_2\theta_2 - r_3\theta_3 - \bar{e}_2 \\ X_3 = r_3\theta_3 - r_4\theta_4 - \bar{e}_3 \\ X_4 = Z_{in} - Z \end{cases} \quad (8)$$

$f_i(t)$ is the nonlinear function of the side clearance of the gear meshing pair, then:

$$f_i(t) = \begin{cases} X_i - \bar{b}_i, & X_i > \bar{b}_i, i = 1, 2, 3; \\ 0, & |X_i| \leq \bar{b}_i, i = 1, 2, 3; \\ X_i + \bar{b}_i, & X_i < -\bar{b}_i, i = 1, 2, 3. \end{cases} \quad (9)$$

The nonlinear function of the reserve clearance of the roller one-way clutch is:

$$f_c(t) = \begin{cases} X_c r_c - b_c, & X_c r_c > b_c \\ 0, & |X_c r_c| \leq b_c \\ X_c r_c + b_c, & X_c r_c < -b_c \end{cases} \quad (10)$$

where r_c is the radius of movement of the one-way bearing roller.

Taking the first harmonic component of the meshing stiffness of the gear meshing pair, the time-varying meshing stiffness is

$$K_i = k_{avi} + k_{mi} \cos(\omega_i t + \varphi_i) \quad i = 1, 2, 3; \quad (11)$$

where $\omega_1 = 4A\omega/p$, p is the tooth pitch of the driving gear in the meshing pair, A is the amplitude of the displacement excitation, and $\omega_i = \mu\omega_1, i = 2, 3$.

In order to solve the problem smoothly, relative coordinates are introduced to eliminate rigid body displacements:

$$\begin{cases} \ddot{X}_1 = \ddot{Z}_{in} - \frac{r_1}{I_1} (r_1 K_1 f_1 + r_1 C_1 \dot{X}_1 - K_c f_c - C_c \dot{X}_c) \\ \quad - \frac{1}{m} (K_4 X_4 + r_1 K_1 f_1 \cos \alpha + r_1 C_1 \dot{X}_1 \cos \alpha) \cos \alpha - \bar{e}_1 \\ \ddot{X}_c = \frac{1}{I_1} (r_1 K_1 f_1 + r_1 C_1 \dot{X}_1 - K_c f_c - C_c \dot{X}_c) - \frac{1}{I_2} (K_c f_c + C_c \dot{X}_c - r_2 K_2 f_2 - r_2 C_2 \dot{X}_2) \\ \ddot{X}_2 = \frac{r_2}{I_2} (K_c f_c + C_c \dot{X}_c - r_2 K_2 f_2 - r_2 C_2 \dot{X}_2) \\ \quad - \frac{r_3}{I_3} (r_3 K_2 f_2 + r_3 C_2 \dot{X}_2 - r_3 K_3 f_3 - r_3 C_3 \dot{X}_3 - T_e) - \bar{e}_2 \\ \ddot{X}_3 = \frac{r_3}{I_3} (r_3 K_2 f_2 + r_3 C_2 \dot{X}_2 - r_3 K_3 f_3 - r_3 C_3 \dot{X}_3 - T_e) - \frac{r_4}{I_4} (r_4 K_3 f_3 + r_4 C_3 \dot{X}_3) - \bar{e}_3 \\ \ddot{X}_4 = \ddot{Z}_{in} - \frac{1}{m} (K_4 X_4 + K_1 f_1 + C_1 \dot{X}_1) \end{cases} \quad (12)$$

Defining the nominal time scale $\omega_c = \sqrt{k_{av1}/m}$, let $\tau = \omega_c t$, $\omega_{hi} = \omega_i/\omega_c$. \ddot{x}_i is the derivative of x_{to} . Using characteristic length b , let $x_i = \frac{X_i}{b}$, $b_i = \frac{\bar{b}_i}{b}$, $e_i(t) = \frac{\bar{e}_i(t)}{b}$, $e_{ai} = \frac{\bar{e}_{ai}}{b}$.

Defining dimensionless parameters:

$$\begin{aligned} \xi_{11} &= \frac{r_1^2 C_1}{I_1 \omega_c} + \frac{C_1 \cos \alpha}{m \omega_c} & K_{11} &= \frac{r_1^2 k_{av1}}{I_1 \omega_c^2} + \frac{k_{av1} \cos \alpha}{m \omega_c^2} & \xi_{1c} &= -\frac{r_1 C_c}{I_1 \omega_c} & K_{1c} &= -\frac{r_1 K_c}{I_1 \omega_c^2} & K_{14} &= \frac{K_4 \cos \alpha}{m \omega_c^2} \\ \xi_{c1} &= -\frac{r_1 C_1}{I_1 \omega_c} & K_{c1} &= -\frac{r_1 k_{av1}}{I_1 \omega_c^2} & \xi_{cc} &= \frac{C_c}{I_1 \omega_c} + \frac{C_c}{I_2 \omega_c} & K_{cc} &= \frac{K_c}{I_1 \omega_c^2} + \frac{K_c}{I_2 \omega_c^2} & \xi_{c2} &= -\frac{1}{I_2 \omega_c} r_2 C_2 & K_{c2} &= -\frac{r_2 k_{av2}}{I_2 \omega_c^2} \\ \xi_{2c} &= -\frac{r_2 C_c}{I_2 \omega_c} & K_{2c} &= -\frac{r_2 K_c}{I_2 \omega_c^2} & \xi_{22} &= \frac{r_2^2 C_2}{I_2 \omega_c^2} + \frac{r_3^2 C_2}{I_3 \omega_c} & K_{22} &= \frac{r_2^2 k_{av2}}{I_2 \omega_c^2} + \frac{r_3^2 k_{av2}}{I_3 \omega_c^2} & \xi_{23} &= -\frac{r_3^2 C_3}{I_3 \omega_c} & K_{23} &= -\frac{r_3^2 k_{av3}}{I_3 \omega_c^2} \\ \xi_{32} &= -\frac{r_3^2 C_2}{I_3 \omega_c} & K_{32} &= -\frac{r_3^2 k_{av2}}{I_3 \omega_c^2} & \xi_{33} &= \frac{r_3^2 C_3}{I_3 \omega_c} + \frac{r_4^2 C_3}{I_4 \omega_c} & K_{33} &= \frac{r_3^2 k_{av3}}{I_3 \omega_c^2} + \frac{r_4^2 k_{av3}}{I_4 \omega_c^2} \\ \xi_{41} &= \frac{C_1}{m \omega_c} & K_{41} &= \frac{k_{av1}}{m \omega_c^2} & K_{44} &= \frac{K_4}{m \omega_c^2} \end{aligned} \quad (13)$$

The dimensionless differential equation of motion for the electrical energy regeneration system is obtained by transforming:

$$\begin{cases} \ddot{x}_1 + \xi_{11}\dot{x}_1 + K_{11}k_1(\tau) f_1(\tau) + \xi_{1c}\dot{x}_c + K_{1c}f_c(\tau) + K_{14}x_4 = p_1(\tau) \\ \ddot{x}_c + \xi_{c1}\dot{x}_1 + K_{c1}k_1(\tau) f_1(\tau) + \xi_{cc}\dot{x}_c + K_{cc}f_c(\tau) + \xi_{c2}\dot{x}_2 + K_{c2}k_2(\tau) f_2(\tau) = 0 \\ \ddot{x}_2 + \xi_{2c}\dot{x}_c + K_{2c}f_c(\tau) + \xi_{22}\dot{x}_2 + K_{22}k_2(\tau) f_2(\tau) + \xi_{23}\dot{x}_3 + K_{23}k_3(\tau) f_3(\tau) = p_2(\tau) \\ \ddot{x}_3 + \xi_{32}\dot{x}_2 + K_{32}k_2(\tau) f_2(\tau) + \xi_{33}\dot{x}_3 + K_{33}k_3(\tau) f_3(\tau) = p_3(\tau) \\ \ddot{x}_4 + \xi_{41}\dot{x}_1 + K_{41}k_1(\tau) f_1(\tau) + K_{44}x_4 = p_4(\tau) \end{cases} \tag{14}$$

Where, $p_1 = \ddot{Z}_{in} - \ddot{e}_1$ $p_2 = \frac{r_3}{l_3 b \omega_c^2} T_e - \ddot{e}_2$ $p_3 = -\ddot{e}_3 - \frac{r_3}{l_3 b \omega_c^2} T_e$ $p_4 = \ddot{Z}_{in}$.

$$f_i(\tau) = \begin{cases} x_i - b_i, & x_i > b_i, i = 1, 2, 3; \\ 0, & |x_i| \leq b_i, i = 1, 2, 3; \\ x_i + b_i, & x_i < -b_i, i = 1, 2, 3. \end{cases}$$

3 Simulation Investigation

Taking the two one-way clutches mechanical electromagnetic power regeneration system as the research object, considering the time-varying meshing stiffness, meshing damping, tooth side clearance, and comprehensive transmission error of the meshing pair, as well as the reserve clearance of the one-way clutch, based on the above differential equation of motion group, using variable step size Runge-Kutta algorithm for the numerical solution of system dynamics [21]. The parameters used in the calculation are shown in Tables 1 and 2.

The bifurcation diagram of the dimensionless displacement of the first-stage bevel gear with the meshing frequency is shown in Fig. 5. It can be seen from Fig. 5 that when the meshing frequency ω is less than 2.56 Hz, the electric energy regeneration system exhibits a stable single-cycle motion. Taking $\omega = 2.02$ Hz as an example, the dimensionless time-domain response diagram, phase diagram, and Poincaré cross-sectional diagram of the first-stage bevel gear are shown in Fig. 6. The movement process of the gear is expressed from the tooth surface meshing to the disengagement then to the tooth surface meshing. When the meshing frequency continues to increase, the single-period motion becomes unstable, and the motion state of the system is transformed into quasiperiodic motion from periodic motion. Taking $\omega = 2.58$ Hz as an example, the dimensionless time-domain response diagram, phase diagram, and Poincaré cross-sectional diagram of the first-stage bevel gear are shown in Fig. 7. The phase diagram is shown as an annular band with a certain width, and the Poincaré cross-section is shown by a circle composed of points. Continue to increase the meshing frequency, and the system motion is transformed from quasiperiodic motion to chaotic motion. Taking $\omega = 4.54$ Hz as an example, the dimensionless time-domain response diagram, phase diagram, and

Table 1 Gear system parameters

Parameter	Symbol	Value	Parameter	Symbol	Value
Battery quality	$m(\text{kg})$	90		z_2	50
Gear shaft quality	$m_1(\text{kg})$	0.6691	Number of bevel gear teeth	z_3	50
Number of rack teeth	z	20		z_4	50
Number of gear shaft teeth	z_1	18		$I_2(10^{-6}\text{kg} \cdot \text{m}^2)$	819.7169
Moment of inertia of gear shaft	$I_1(10^{-6}\text{kg} \cdot \text{m}^2)$	56.5730	Bevel gear moment of inertia	$I_3(10^{-6}\text{kg} \cdot \text{m}^2)$	2050.2
Gear shaft radius	$r_1(\text{m})$	0.018		$I_4(10^{-6}\text{kg} \cdot \text{m}^2)$	819.7169
One-way clutch damping	$C_c(\text{N} \cdot \text{m} \cdot \text{s}/\text{rad})$	400		$r_2(\text{m})$	0.05
One-way clutch stiffness	$K_c(\text{N} \cdot \text{m}/\text{rad})$	3.5×10^4	Bevel gear radius	$r_3(\text{m})$	0.05
One-way clutch clearance	$b_c(\text{m})$	8×10^{-6}		$r_4(\text{m})$	0.05
Gear rack clearance	$b_1(\text{m})$	5×10^{-6}	Bevel gear meshing clearance	$b_2b_3(\text{m})$	2×10^{-6}

Table 2 Generator parameters

Parameter	Value
Generator rotor inertia	$0.4 \times 10^{-4} \text{ kg} \cdot \text{m}^2$
Internal resistance	0.45Ω
External load	5Ω
Back electromotive voltage constant	$0.0458 \text{ V} \cdot \text{s}/\text{rad}$
Speed increaser transmission ratio	1:10

Poincaré cross-sectional diagram of the first-stage bevel gear are shown in Fig. 8. The Chaotic motion causes the unstable vibration of the electric energy regeneration system.

4 Conclusions

A mechanical electromagnetic energy regeneration device using two one-way clutches is proposed to extend the range of electric vehicles. The transmission system converts the bidirectional vibration of the rack into unidirectional rotation of the input shaft of the generator, which greatly increases reliability and efficiency. The generator will be driven in one direction to convert the kinetic energy into electrical energy. Nonlinear parameters in the energy regeneration device will affect

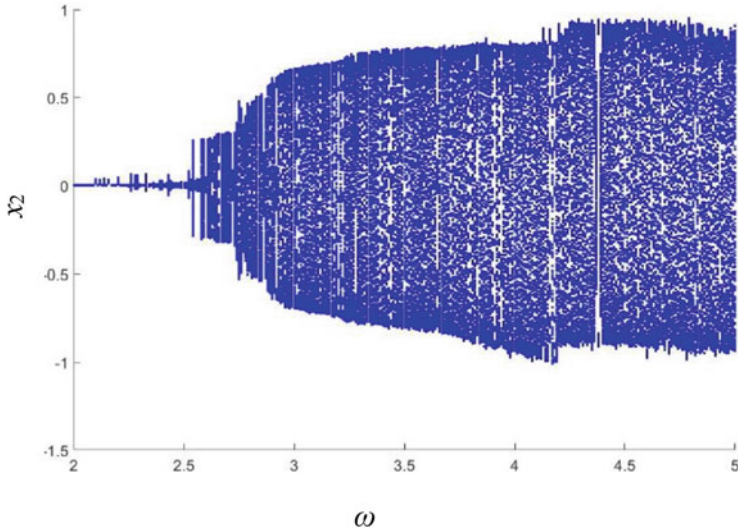


Fig. 5 Bifurcation diagram of the system changing with the meshing frequency

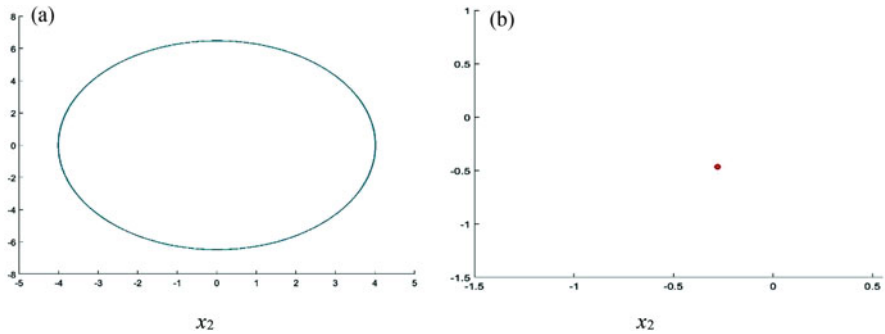


Fig. 6 Phase diagram (a) and Poincaré cross section (b) ($\omega = 2.02$ Hz)

the stability of the system and the efficiency of electric energy regeneration. Through the analysis of the nonlinear parameters in the device, considering the time-varying mesh stiffness, mesh damping, backlash and dynamic transmission error of the meshing pair, and the reserve clearance of the one-way clutch, using the mass centralized method to establish the multiple degrees of freedom nonlinear dynamic model. The Runge-Kutta method is used to calculate the nonlinear differential equation. The time-series response chart, kinematic phase diagram, Poincare map, and bifurcation diagram are used to analyze the influence of parameters. The results show that as the meshing frequency changes, the system response changes from period-doubling bifurcation to chaotic motion. In addition, The influence law of parameters on the damping characteristics of the device is revealed. The research results can improve the stability and the efficiency of electric energy regeneration

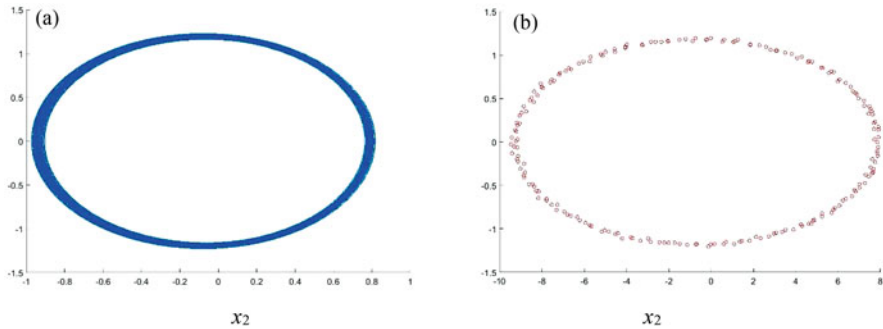


Fig. 7 Phase diagram (a) and Poincaré cross section (b) ($\omega = 2.58$ Hz)

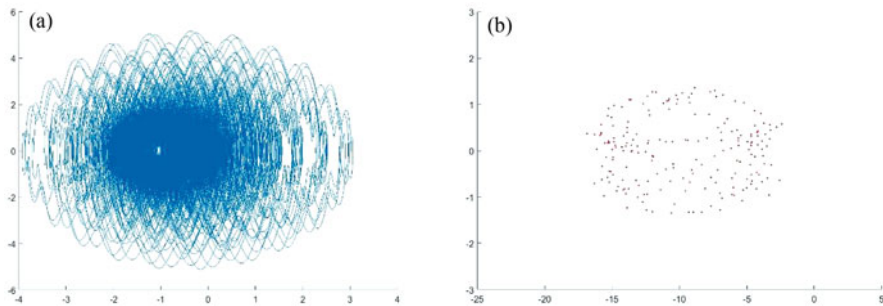


Fig. 8 Phase diagram (a) and Poincaré cross section (b) ($\omega = 4.54$ Hz)

devices and achieve the goals of prolonging the cruising mileage. It can lay a profound theoretical foundation and reality significance for the research of electric energy regeneration devices.

Acknowledgments This study was funded by the National Key Research and Development Program of China (grant number 2016YFD0700800), and the International Cooperation Project of Qilu University of Technology (grant number QLUTGJHZ2018022). The authors would like to appreciate all the authors listed in the references, and would also like to thank the funding organizations that provided financial support and anonymous reviewers for helpful comments and suggestions. The authors declare no potential conflicts of interest with respect to the research, authorship, and/or publication of this article.

References

1. Z. Zhang et al., A high-efficiency energy regenerative shock absorber using supercapacitors for renewable energy applications in range extended electric vehicle. *Appl. Energy* **178**, 177–188 (2016)
2. H. Taghavifar, A novel energy harvesting approach for hybrid electromagnetic-based suspension system of off-road vehicles considering terrain deformability. *Mech. Syst. Signal Process.* **146**, 106988 (2021)

3. R. Zhang et al., A comprehensive comparison of the vehicle vibration energy harvesting abilities of the regenerative shock absorbers predicted by the quarter, half and full vehicle suspension system models. *Appl. Energy* **272**, 115180 (2020)
4. M.A.A. Abdelkareem et al., Vibration energy harvesting in automotive suspension system: A detailed review. *Appl. Energy* **229**, 672–699 (2018)
5. S. Li et al., Energy-harvesting variable/constant damping suspension system with motor based electromagnetic damper. *Energy* **189**, 116199 (2019)
6. R. Tavares, M. Ruderman, Energy harvesting using piezoelectric transducers for suspension systems. *Mechatronics* **65**, 102294 (2020)
7. A. Genovese, S. Strano, M. Terzo, Design and multi-physics optimization of an energy harvesting system integrated in a pneumatic suspension. *Mechatronics* **69**, 102395 (2020)
8. X. Wang, Stability research of multistage gear transmission system with crack fault. *J. Sound Vib.* **434**, 63–77 (2018)
9. J. Chen et al., Study on reliability of shearer permanent magnet semi-direct drive gear transmission system. *Int. J. Fatigue* **132**, 105387 (2020)
10. K. Huang et al., Bifurcation and chaos analysis of a spur gear pair system with fractal gear backlash. *Chaos, Solitons Fractals* **142**, 110387 (2020)
11. Y. Yang et al., Nonlinear dynamic response of a spur gear pair based on the modeling of periodic mesh stiffness and static transmission error. *Appl. Math. Model.* **72**, 444–469 (2019)
12. W. Xiao et al., Effect of particle damping on high-power gear transmission with dynamic coupling for continuum and non-continuum. *Appl. Acoust.* **173**, 107724 (2021)
13. L.-Y. Zhu, J.F. Shi, X.F. Gou, Modeling and dynamics analyzing of a torsional-bending-pendular face-gear drive system considering multi-state engagements. *Mech. Mach. Theory* **149**, 103790 (2020)
14. D. Shin, A. Palazzolo, Nonlinear analysis of a geared rotor system supported by fluid film journal bearings. *J. Sound Vib.* **475**, 115269 (2020)
15. Y. Yi et al., Nonlinear dynamic modelling and analysis for a spur gear system with time-varying pressure angle and gear backlash. *Mech. Syst. Signal Process.* **132**, 18–34 (2019)
16. C.H. Chin et al., Durability assessment of suspension coil spring considering the multifractality of road excitations. *Measurement* **158**, 107697 (2020)
17. X. Shao et al., Coupling effect between road excitation and an in-wheel switched reluctance motor on vehicle ride comfort and active suspension control. *J. Sound Vib.* **443**, 683–702 (2019)
18. B. Huang et al., Development and optimization of an energy-regenerative suspension system under stochastic road excitation. *J. Sound Vib.* **357**, 16–34 (2015)
19. J. Yao et al., Analysis of the stability of nonlinear suspension system with slow-varying sprung mass under dual-excitation. *J. Sound Vib.* **425**, 124–136 (2018)
20. V. Roda-Casanova, F. Sanchez-Marin, Contribution of the deflection of tapered roller bearings to the misalignment of the pinion in a pinion-rack transmission. *Mech. Mach. Theory* **109**, 78–94 (2017)
21. D. Wei et al., Chaos vibration of pinion and rack steering trapezoidal mechanism containing two clearances. *Mech. Syst. Signal Process.* **92**, 146–155 (2017)